

**Nearshore waves and littoral drift along a micro-tidal wave-dominated coast having comparable wind-sea and swell energy**

**Jesbin George, V. Sanil Kumar\*, R. Gowthaman, Jai Singh**

Ocean Engineering Division, CSIR-National Institute of Oceanography (Council of Scientific & Industrial Research), Dona Paula-403 004 Goa India

\* Correspondence: sanil@nio.org

**Abstract**

The nearshore wave characteristics and variations in littoral drift (longshore sediment transport; LST) estimated based on different approaches for four years along the Vengurla coast having comparable wind-sea and swell energy are assessed. The waverider buoy measured data at 15-m water depth is utilised as the input wave parameters along with the reanalysis model data, and the numerical wave model Delft-3D is used for estimating the nearshore wave parameters. The relative contribution of wind-seas and swells on LST rates are specifically examined. The clear prevalence of west-southwest waves implies the prevalence of south to north longshore sediment transport with net transport varying from  $0.19 - 0.37 \times 10^5 \text{ m}^3/\text{yr}$ . LST is strongly dependent on the breaker angle and a small change in the wave direction substantially alters the LST, and hence reanalysis/model data with coarse resolutions produce large errors (~38%) in the LST estimate. The annual gross LST rate based on integral wave parameters is only 58% of that considering the wind-seas and swells separately since the wind-sea energy is comparable to swell energy, and the direction of these two systems differ significantly.

**Keywords:** coastal processes; longshore sediment transport; nearshore modelling; swells; wave characteristics; wind-seas

## 1. Introduction

Coastal zone is the most dynamic region due to the release of energy by the surface gravity waves (hereafter waves). The waves propagating into the shallow water transforms due to reflection, refraction, bottom friction, shoaling and breaking. When refracted, oblique waves reach the shore; the alongshore wave energy flux induces a net sediment transport whose gradients are responsible for shoreline evolution [1]. Breaking waves in the surf zone make an additional sediment stirring effect, caused by the breaking-induced flows, enhanced turbulent kinetic energy in the water column, and pore pressure responses in the sediments [2]. Knowledge of the physical processes in the nearshore region that impact sediment transport is essential to understand the erosion/accretion processes that mainly regulate the coastline stability [3]. Substantial morphological changes occur in the sandy beaches due to the action of waves, currents, and tides, often controlled by the height and length of the nearshore waves. This morpho-dynamic change can be observed on a different timescale and may vary from daily, monthly and even yearly. The temporal variations in the littoral system are observed due to variations in the wave climate, and the change in the direction of longshore sediment transport (LST) is mainly due to change in the wave direction [4]–[6]. The wave direction can vary due to the changes in the offshore wave climate or because of the variations in the nearshore bathymetry [7]–[9]. Quantitative processes and coastal evolution through numerical modelling is now possible due to the significant advances in understanding the physical processes and mathematical modelling techniques over the last few years [8]. One-dimensional morphology evolution models consider sediment transport along the longshore dimension based on several simplifying assumptions. The joint application of a calibrated wave propagation model, the LST equation and the one-line model constitutes a management tool for predicting the evolution of these complex coastal settings [5]. Bergillos et al. [6] used an integrated methodology to predict the plan view response of a deltaic coast (Guadalfeo, southern Spain) over a two-year period forced by different nourishment scenarios of coastline morphology, input LST and nourished sediment size.

During the past few decades, several methods have been developed for the computation of LST, and most of them are the bulk transport formulas; explicit equations based on simplified representations of physical processes and depends on the empirical coefficients. Bulk transport methods provide an estimate of the integrated LST rate (LSTR) over the whole profile with few input parameters. Many studies [10–12] indicate that transport is proportional to the energy flux of the longshore component of wave power for fully developed transport conditions. Komar and Inman [13] used the field measured waves and found that the immersed weight of LSTR is directly proportional to the longshore component of wave energy flux. Smith et al. [14] reported that the LST estimation using

Coastal Engineering Research Centre (CERC) [15] has an accuracy of about 30-50% and also the coefficient  $K$  of 0.39 is found to overestimate the LSTR by 7 to 8 times for spilling breakers and more than a factor of three for plunging breakers. Chempalayil et al. [16] studied various empirical equations and they found that the CERC equation shows a similarity in two locations having different nearshore characteristics, whereas, the equation proposed by Walton Jr and Bruno [17] and Kamphuis [18] resulted to a vast difference in the values of LSTR due to the change in the nearshore parameters. Samaras and Koutitas [19] performed a review on studies regarding the comparative analysis and evaluation of the efficiency of 18 LST rate formulae and reported that Kamphuis (1991) formula performed well against laboratory measurements. They also intercompared CERC formula, the Bayram et al. [20] formula and the Kamphuis [18] formula as part of a properly adapted 1-D shoreline evolution model.

Shanas and Kumar [4] and Kumar et al. [21] studied four bulk formula (CERC, Kamphuis, Walton & Bruno and Komar) for the estimation of LSTR with the nearshore wave parameters based on wave transformation model Delft-3D as input and they observed that the estimation based on Kamphuis is close to the measured values. Prediction effect of the CERC formula gradually decreases from the open coast to the sheltered zone, whereas the Kamphuis approximation is reasonable for all types of coastal zones. The LSTR at different locations along the west coast of India based on measured wave data has been investigated by various researchers and reported to be between  $1.4 \times 10^5$  and  $7.0 \times 10^5$   $\text{m}^3/\text{yr}$  (Table 1). The LSTR estimate based on the Kamphuis [18] formula, which includes all the responsible parameters like the wave period, beach slope, and sediment grain size is found to be a reliable estimate for the west coast of India [4, 16]. Hence the same is used in the present study.

Studies conducted in the eastern Arabian Sea indicate that due to the co-existence of swells and wind-seas, the wave spectrum is bimodal during most of the time [22–24]. The predominance of wind-seas and the swells were also reported in the eastern Arabian Sea [25]. In most of the studies, the integral wave parameters resulting from the combined wind-seas and swells are used in the estimation of the LSTR along with the wave direction corresponding to the spectral peak [4, 16, 21]. But in areas like the eastern Arabian Sea, where the wind-seas and swells have different directions [24], the estimation based on LSTR considering the wind-seas and swells separately needs examination. Also, it is essential to understand changes in the nearshore wave climate and LST in an annual cycle as the nearshore regions up to 10 km from the coast in the eastern Arabian Sea is an intense fishing zone and this area is also extensively used for tourism-related activities and development of marine facilities. The relative contribution of wind-seas and swells on LSTR are not specifically examined in all previous studies and the LSTR estimate is based on the integral wave parameters. To best of our

knowledge, no previous studies were done along this region to estimate LST and wave climate using continuously measured data for more than a year. Thus the present study aims to understand the changes in the nearshore wave parameters and the LSTR and investigates the influence of wind-seas and swells on the LST.

## **2. Study area**

The west coast of India is subjected to high wave activity during the Indian summer, i.e., southwest monsoon (June-September, hereafter monsoon) and during this period most of the sandy beaches undergo erosion [29]. Typically, the beach restores its equilibrium state during the post-monsoon period [28]. The study area is off Vengurla situated along the central west coast of India (location 15.87° N to 73.63° E) (Figure 1). The east side of this coastal segment is bounded by the Western Ghats mountain range, while the Arabian Sea extends along its west side. It is surrounded by a semi-circular range of hills and is exposed to open ocean waves from north-west to south; The nearest landmass is ~1500 km in the north-west, ~2000 km in the west, ~4000 km southwest and ~9000 km in the south [30]. Vengurla coast is characterised by the tropical climate, and the annual precipitation is ~ 3100 mm [31]. Nature and spatial distribution of geomorphic features along the coast indicate that the study area is a scene of neotectonic activity [32]. The tidal regime of this region is 2.3 m during spring tide and 1.3 m during neap tide. The longshore current velocity of 0.5 m/s was reported [31]. High wave activity (seasonal average  $H_s \sim 2$  m) is experienced during monsoon and calm wave conditions ( $H_s < 1$  m) during the remaining period of the year [25]. Based on Davies classification [33, 34], the wave and tide data together exhibit that the study area is on a micro-tidal wave-dominated coast and the predominant breaker is plunging breaker with multiple breakers [35].

## **3. Data and Methods**

The bathymetry of the study area is obtained by merging the nearshore measured bathymetry data from coast to 5 m water depth with the digitised naval hydrographic chart No. 2043 [36]. During September 2014 to August 2015, the median size of the nearshore sediment ( $D_{50}$ ) is obtained in a monthly interval. The  $D_{50}$  is extracted by the following geometric (modified) Folk and Ward [37] graphical measures using GRADISTAT: a grain analysis package [38] and the size distribution of sediments is obtained using an electromagnetic sieve shaker. Wave data is collected at 30 minutes interval at 15-m from September 2014 to August 2018 and is used as an input for the model. The WAVE module of the Delft3D model [39] is used as the numerical model for nearshore wave transformation to estimate the breaker wave parameters. This numerical model is based on the SWAN model [40], a third-generation phase-averaged wave model based on fully spectral representation of

the action balance equation and it accurately reproduce the main wave propagation processes in coastal areas, i.e., shoaling, refraction due to bottom and current variations, transmission/ blockage through/by obstacles; white capping; bottom friction, depth-induced wave breaking; non-linear wave-wave interactions and wind effects [41]. This model was previously employed along several locations in the central west coast of India [4, 19, 26, 42] and they have described in detail about the wave transformation model, grid generation, attributes, input parameters etc., and is same for the present study. Significant wave height ( $H_s$ ), mean wave direction and mean wave period ( $T_{m02}$ ) are the input wave parameters used in the model. Other input variables used in the model are JONSWAP bottom friction coefficient ( $0.067 \text{ m}^2 \text{ s}^{-3}$  [43]), depth induced breaking (Alpha (1) and Gamma (0.73), [44]), and nonlinear triad interactions (Alpha and Beta being 0.1 and 2.2 respectively) based on Lumped Triad Approximation model [45]. The model simulations are carried out in stationary mode and have three boundaries: (1) open boundary to the west (2) closed boundary to the east and (3) lateral boundaries to the north and south. The model has 24 frequencies between 0.05 – 1 Hz and the directional resolution of the model is 10 degrees. No wind fields were included in the model since the domain is small. Also sea level changes due to the influence of tide is also not considered. The domain is divided into 200 x 450 grid points with a grid spacing of 20 m each along x and y directions. The method suggested by Portilla et al. [46] is used to separate wind-seas and swells from the measured data. The 1-D separation algorithm is on the assumption that the energy at the peak frequency of a swell cannot be higher than the value of a Pierson-Moskowitz (PM) spectrum with the same frequency. If the ratio between the peak energy of a wave system and the energy of a PM spectrum at the same frequency is above a threshold value of 1, the system is considered to represent wind-sea, else it is taken as swell. A separation frequency  $f_c$  is estimated following Portilla et al. [46] and the swell and wind-sea parameters are obtained for frequencies ranging from 0.025 Hz to  $f_c$  and from  $f_c$  to 0.58 Hz, respectively. The 4-years of simulations carried out in a workstation (HP Z 800) took a period of 2 months and the output is stored to a 500 GB hard disk. ERA-Interim data [47] from September 2014 – August 2015 of significant wave height (SWH), mean wave period and mean wave direction at the six-hour interval is also obtained with a spatial resolution of  $0.5^\circ \times 0.5^\circ$  to compare the LSTR estimated with the measured and reanalysis data. For wave transformation based on ERA- I data, the domain was first divided into 400 x 250 points with a grid spacing of 100 m and 75 m respectively. This low - resolution grid is nested to high - resolution grid (450 x 450) with a grid spacing of 10 m each along x and y direction. The model simulation is carried out for four years from 1 September 2014 to 31 August 2018, and the transformed breaking characteristics were extracted by considering the breaking criteria ( $H_b/h_b = 0.78$ ; [15]) This extracted output parameters, breaking wave height ( $H_b$ ),  $T_{m02}$  and wave breaking angle, are used for the calculation of LSTR.

The LST is estimated based on the bulk transport formula developed by Kamphuis [18]. The Kamphuis equation includes the wave period, which influences wave breaking and grain size, which affects the sediment motion. Due to the orientation of coastline at 22° with respect to the west, the wave direction less than 248° generate northerly LST and is taken as positive and wave direction more than 248° generate southerly LST and is taken as negative.

$$Q_{LST} = 7.3H_b^2 T_p^{1.5} m_b^{0.75} d_{50}^{-0.25} \sin^{0.6}(2\theta) \quad (1)$$

Where,  $Q_{LST}$  is the longshore sediment transport in volume per unit time,  $H_b$  = breaking wave height (m),  $T_p$  = peak wave period (s),  $m_b$  = slope of the bottom in the surf zone,  $d_{50}$  = sediment median grain size (mm),  $\theta$  is the angle between the incident wave ray and local shoreline (deg).

## 4. Results and discussion

### 4.1. Wave Characteristics at 15 m water depth

As expected, high waves are observed during the monsoon since the Arabian Sea is the key region of strong air-sea interaction associated with the monsoon. The highest  $H_s$  observed (~ 5 m) is in June 2015 and July 2018, and during the monsoon,  $H_s$  ranged from 0.5 to 5 m with an average value of 1.8 m (Figure 2a) and are predominantly from west - southwest direction (Figure 3) due to the dominance of swells in the west coast of India during this season [21, 48].  $T_{m02}$  during monsoon varies from 3.4 to 9.7 s with an average value of 6.2 s (Figure 2b) and Peak wave period ( $T_p$ ) ranges from 3.8 to 20 s with an average value of 10.5 s (Figure 2c). During February-May (pre-monsoon), waves from northwest (wave direction > 248°) are observed (Fig. 2d) and is predominant during 19.4% of time (Fig 3) and these waves are with  $H_s$  ranging from 0.25 to 2.86 m,  $T_{m02}$  ranging from 4.5 to 8.5 s and  $T_p$  ranging from 2.2 to 22.2 s. During the post-monsoon season (October- January) waves mostly approach from the southwest (Fig 3) with  $H_s$  varying from 0.2 m to 2.5 m,  $T_{m02}$  from 2.5 - 9.6 s and  $T_p$  from 2.1 – 22.2 s. This seasonal distribution of waves indicates that study region has 3 wave regimes; i) swells ( $T_p > 10$  s) from the southwest, ii) wind-seas ( $H_s < 1.5$  m &  $T_p < 8$  s) from the northwest and iii) westerly waves during monsoon ( $H_s > 1.5$  m) (Figure 3).

Highest  $H_s$  of about 2 m along the study region during non-monsoon months was previously reported by Amrutha et al.[25] and the existence of long - period waves ( $T_p > 18$  s) along the eastern Arabian sea was reported by Amrutha et al. [49].  $T_{m02}$  values observed off Vengurla is similar to the value (7 - 8 s) observed off the Goa coast [46]. During the study period, 71% of the waves are with  $H_s$  less than 1 m and 2% of the waves are with  $H_s$  more than 3m. The annual average value of  $H_s$  during the four - yearly cycles (2014-2015, 2015-2016, 2016-2017, 2017-2018) are 0.94, 1.02, 0.95 and 1.01

respectively, indicating an inter-annual variation of up to 8%. However, no significant variations in annually averaged values of  $T_{m02}$  (5.1, 5.3, 5.3 and 5.1 s) and  $T_p$  (11.6, 11.8, 11.6 and 11.3 s.) were observed during different annual cycles.

The surface height variance at the study area is separated into wind-seas and swells (see data and methodology) and the resulting wave height, mean wave period and wave direction of wind-seas and swells for different months during different annual cycles are presented in Table 2 and Table 3 respectively. The monthly average swell  $H_s$  varies from 0.24 to 2.23 m, whereas the monthly averaged wind-sea  $H_s$  varies from 0.21 to 1.17 m. Wave period and direction for both wind- sea and swells are observed to be somehow consistent, and their variation is observed to be less than 3% annually for different months. Most importantly, the wind-sea  $H_s$  is comparable to swell  $H_s$  during non- monsoon seasons (Tables 2 and 3).

During most of the time, the wave spectrum in the study area consists of multiple peaks except in the monsoon with considerable energy in the secondary peak (Figure 4). The wave direction corresponding to both the primary and the secondary peak are also different. Hence, the spectral energy density at the primary peak and the secondary peak are compared separately for the monsoon and non-monsoon period (Figure 5). At both the water depths (15 and 5 m) during the monsoon, the spectral energy density at secondary peak is ~40% of that in the primary peak. During the non-monsoon period, the energy at the secondary peak is 49% (28%) of that in the primary peak at 15 m (5 m) water depth. There is a significant difference between the direction of the wind-sea and the swells, especially during the non-monsoon months at both 15-m and 5-m water depth (Figure 4).

#### **4.2. Model validation and comparison**

The performance of the Delft-3D WAVE module is assessed by comparing the model results with the measured data at 5-m water depth from September 2014 to June 2015 and August 2015. The output parameters from the numerical wave model which are used as input to the LSTR estimate are significant wave height, peak wave period and wave direction. Hence, these parameters are compared with the measured buoy data at 5 m water depth. The skill of the model is determined based on the amount of deviation which is measured by root-mean-square error (RMSE) and bias, between the model results and the observational data and the correlation coefficient (R). The comparison of the measured and simulated wave parameters at 5-m water depth for both non-monsoon and monsoon seasons are presented in Fig. 6. During non-monsoon season,  $H_s$  shows a bias of -0.012 m and RMSE of 0.063 m and the correlation coefficient (R) is 0.93. On the other hand, the bias, RMSE and R values of the mean wave period ( $T_{m02}$ ) and wave direction during non-monsoon are -1.26 s, 1.55 s, 0.73 and

3.7°, 19.7°, 0.44 respectively. During monsoon, the bias, RMSE and R values for  $H_s$  are 0.041 m, 0.22 m, and 0.91 respectively and for  $T_{m02}$  and wave direction, the values are -0.77 s, 1.03 s, 0.77 and -0.06°, 9.42°, 0.65 respectively. It is observed that both  $H_s$  and  $T_{m02}$  under predicts ~18% during monsoon and 16 and 23% during non- monsoon, whereas direction under predicts less than 2% during both seasons. During the non-monsoon period, when the wind-sea is stronger and close to the swell energy, the comparison between the wave direction between the model and the measured data show large scatter. The performance of the model using the separated swell and wind-sea has also been compared with the measured data (Figure 6) and is presented in Table 4. Kumar et al.[21] observed that the Delft-3D wave module [17] results are comparable (RMSE~0.067 m, bias~0.017 m and SI~0.083) with the measured data at a water depth of 2.5 m.

### 4.3 Breaker characteristics

During the post-monsoon season, breaker heights ( $H_b$ ) less than 1 m are observed (Figure 7a). Along the study region, Chandramohan et al. [51] observed breaker heights of about 0.7 m and mean wave periods of 5-8 s during non-monsoon seasons. There is a considerable increase in the wave height to about 2 m during the monsoon with its peak around 3.8 m during 2015 (Figure 7a). During the study period, about 69% of the wave height is less than or equal to 1 m and during 17% of the time,  $H_b$  exceeded 1.5 m (Figure 7a). Off the central west coast of India, Shanas and Kumar [4] observed that during an annual cycle, 0.6-1.1 m waves occurred for about 55% of the time. Wave period at the breaker zone generally varies in the range of 2.7 – 9.6 s with an average value of 4.4 s. (Figure 7b). Also, Fig 7c clearly shows that the breaker angle decreased during the monsoon period and is high during the non-monsoon season. The frequency distribution indicates that around 19% of waves break at angles more than 20° and 44% of waves breaks at an angle less than 10°. About 74% time breaker angle is directed towards the north. The predominance of northerly directed waves in the eastern Arabian Sea were previously reported by Jesbin et al. [42].

### 4.4 LSTR estimate based on integral wave parameters

LST rates along the Vengurla coast during different months of four annual cycles were estimated using Eq. 1 Estimated LSTR is low during the non-monsoon period due to small breaker heights (Table 5). The annual gross LSTR ranges from 0.59 - 0.74 x 10<sup>5</sup> m<sup>3</sup>/yr for the study region. The gross LSTR for a region ~140 km north of the study area is 0.4 x 10<sup>5</sup> m<sup>3</sup>/yr [26]. Shanas and Kumar [4] and Kumar et al. [21] along Kundapura and Malpe coasts estimated LST using Kamphuis equation and reported an LSTR of 1.63 x 10<sup>5</sup> m<sup>3</sup>/yr and 8.9 x 10<sup>5</sup> m<sup>3</sup>/yr respectively indicating that there is large variations in the gross LSTR within 440 km stretch along the central west coast of India. Chandramohan and Nayak [52] have reported that south Maharashtra coast has negligible annual net



LSTR. The monthly pattern shows that net LSTR varied from 13 (in February) to 19993 (in June)  $\text{m}^3/\text{month}$  (Table 5). Previously along the study region, based on visual observations of breaker heights and period, Chandramohan et al. [53] estimated a southerly directed net LSTR of  $0.53 \times 10^5 \text{ m}^3/\text{yr}$ . Recently, Noujas et al. [27], using LITDRIFT model estimated LSTR of  $1.18 \times 10^5 \text{ m}^3/\text{yr}$  along Vengurla coast with an annual net value ranging from -7778 to -9015  $\text{m}^3/\text{yr}$ . The annual net value for the present study is observed to be ranging from 0.26 to  $0.37 \times 10^5 \text{ m}^3/\text{yr}$ , and the transport is towards the north. The direction of sediment transport is predominantly towards the north from June to September (Figure 7d) which is due to the predominance of south-westerly swell waves (Figure 3) along this region. However, large southerly LST rates are observed during 2015 monsoon which is associated with high breaker heights (Figure 7a) and southerly breaker heights (Figure 7c). During the pre-monsoon, sediment transport is predominantly observed to be southerly with low magnitude. The longshore current is responsible for the directional change during the monsoon, and the seasonal wind pattern is responsible for the change in the direction of LSTR during non-monsoon.

Variation of LSTR with the  $H_s$  indicates that the LST increases with an increase in the wave height and decreases with the reduction of wave height (Figure 8). LST rates are influenced mainly by the breaker parameters [14]. The influence of breaker height on LSTR for different seasons is studied through a scatter plot between these two parameters during the annual cycle 2014-2015 (Figure 8). The breaker height is high during the monsoon and is of order 1 to 2 m, and also the LSTR is high during this season. Wave breaker angle is low during the monsoon, whereas the sediment transport is high during this time (Figure 8). Noujas et al [27] examined the sensitivity analysis of net LSTR by increasing the wave height contribution by 10% and observed an increasing trend in LSTR. Recently, Jesbin et al. [26] investigates the influence on variations in LSTR due to errors in breaking angle and breaker height and observed that they are sensitive to LST rates and could lead to large errors in their estimation. There is a high variability of LSTR during the monsoon season. The annual gross LST for 5, 10, 15 and 20% increase in the  $H_s$  values are 71933, 78961, 86427 and 94322  $\text{m}^3/\text{yr}$ . A 5, 10, 15 and 20% increase in the  $H_s$  value results in 10, 21, 32 and 44% increase in the annual LST. Even though the waves are influenced by the sea breeze during the pre-monsoon period, the influence of sea breeze on LST is negligible (Figure not shown) since the LST depends on both the wave height and wave period and these two parameters have an inverse relationship during the sea breeze period [54].

#### **4.5 LSTR estimate based on wind-sea and swells**

As discussed in section 4.1, wind- seas and swell along the study region is comparable during non-monsoonal months. Thus LSTR based on the separated wind –seas and swells were estimated along the study region from September 2014 – August 2015 (Table 6). Monthly gross LSTR based on

wind-sea varies from 244 m<sup>3</sup>/month (in November) to 3232 m<sup>3</sup>/month (in June), whereas that based on swell varies from 1461 m<sup>3</sup>/month (in February) to 23018 m<sup>3</sup>/month (in June). The wind-sea contribution to the monthly gross LSTR varies from 6 to 25% with the lowest in March and the highest in June. The bulk (75 to 94%) of the gross LSTR is due to swells (Table 6). Based on remote sensing techniques, Kunte and Wagle [55] reported that sediment transport direction along the Maharashtra coast is bi-directional and seasonal dependent.

From Table 6, it is evident that wind seas generally contribute to southerly net transport of LST, whereas, swells contribute to northerly net LST. The annual gross LSTR due to wind-seas is  $0.149 \times 10^5 \text{ m}^3$  and that due to swells is  $0.987 \times 10^5 \text{ m}^3$ . The annual gross LSTR based on bulk wave parameters ( $0.6534 \times 10^5 \text{ m}^3/\text{y}$ ) is only 58% of that considering the wind-seas and swells ( $1.13632 \times 10^5 \text{ m}^3/\text{y}$ ). The gross transport during the pre-monsoon, monsoon and post-monsoon period is 13, 70 and 17% of the annual transport. Similarly the net transport during the pre-monsoon, monsoon and post-monsoon period is 10, 78 and 12%. The LSTR based on integral wave parameters is least (37 to 47%) of that based on relative contribution of wind-seas and swells during November to May, when both wind-seas and swells are coexists in the area. During monsoon, when swells dominates, the LSTR based on integral wave parameters is 64 to 66% of that based on relative contribution of wind-seas and swells. For incoming west-southwesterly wave conditions, which are predominantly swells, the LSTR is generally higher due to higher spectral peak periods and higher significant wave height (Fig. 8e). For incoming north-westerly waves, which are predominantly wind-seas, the LSTR is lower due to lower wave periods and lower significant wave heights. The study shows that in regions where there is large difference in the direction of the wind-seas and swells, considering the integral parameters will lead to errors in the LSTR estimate. Studies of this type, involving model calibration based on field measurements, considering relative contribution of wind-seas and swells are deemed to provide a useful perspective on the LSTR to be applied for coastal engineering applications and morphological studies.

#### **4.6 LSTR estimate based on ERA-Interim data**

In most of the locations, the measured wave data is not available. Thus the researchers use the reanalysis data such as ERA-Interim or ERA-40 [56] produced by the European Centre for Medium Weather Forecasts for estimation of the LSTR. Many researchers across the globe have used these datasets to estimate the LST rates [42, 57] and to understand the physical mechanism driving the wave climate [58]. For e.g, temporal variations in annual net LST rates were examined using ERA data sets along the Southeast Queensland, Australia and were linked to climate indices [57]. Along the west coast of India, Jesbin et al. [42] and Chowdhury et al. [59] estimated temporal variations in LST

using ERA data sets and established a link with pacific climate variability and the latitudinal position of the inter-tropical convergence zone (ITCZ) respectively. Hence, we have compared the LSTR estimate based on ERA-Interim with the buoy measured wave data. The monthly gross and net LSTR shows a large difference in the LSTR estimate based on ERA-Interim data compared (Table 6) to that based on measured buoy data (Table 5).

The large difference in the LSTR between the two estimations is due to the large difference in the wave period and wave direction between the two datasets (Figure 9). Breaker height from ERA-Interim  $H_s$  can be estimated with an RMSE of 0.29 m for the study area, but the wave direction shows large scatter (up to  $17^\circ$ ) (Figure 9). Even a 20% increase in the  $H_s$  value results in a 44% increase in the annual LST [24]. Earlier study [60] shown that ERA-Interim wave period is close to the energy wave period ( $T_e = m_{-1}/m_0$ ) and not the mean wave period of the buoy data and hence, there is large scatter between the mean wave period of the buoy measured data and the ERA-Interim data (Fig. 9). The large difference in the wave direction is due to the fact that ERA-Interim data is based on a low-resolution global model ( $0.70^\circ$  for the atmospheric model and  $1^\circ$  for the ocean model [43]) and also the measurements are made in the nearshore environment. Another reason for the substantial difference between the wave direction of the ERA-Interim and the buoy data is due to the predominance of wind-seas and swells in the study area. During the non-monsoon period, in some of the instances, the spectral energy of the wind-sea peak and the swell peak have comparable energy, and during this period, the direction of the wind-sea and swell have large difference (Figure 5). In some cases, the ERA-Interim data shows the swell direction, whereas the measured data represent the wind-sea direction, whereas, in other instances, vice versa is observed (Figure 10). Also, the short-term sub-synoptic scale wind pulses and fluctuations are not likely to be captured by a lower resolution ERA-Interim data [42, 60]. Hence, datasets like ERA-Interim solely cannot be used for studying the nearshore processes, especially for estimating the LSTR without validation.

## 5. Conclusions

The present study examines the wave characteristics and longshore sediment transport rate (LSTR) for four different annual cycles along the Vengurla coast. The wave data collected at 15-m water depth at 1-hour interval is used, and the nearshore wave parameters are estimated using a numerical model Delft 3D Wave module and compare the results with field measured data from a buoy, thus derived parameters are employed for estimating LSTR. The model results show good agreement with the measured data. Annually,  $H_s$  observed to be varying up to 8% whereas, mean wave period and peak wave period shows no significant inter-annual variations. The study area has three wave regimes; swells from the southwest, wind-seas from the northwest and westerly waves during the

monsoon and has a comparable wind-seas and swells. Gross LSTR along the region is high during monsoon and during non- monsoon period, LSTR is of low magnitude and varies annually in the range of  $0.59 - 0.74 \times 10^5 \text{ m}^3/\text{yr}$ . LST direction depends on the breaker direction and is predominantly northward and hence the monthly net LSTR is towards the north in all months, but the estimate based on ERA-Interim reanalysis data produce southerly LST in January, July and August. A small error in the breaker angle induces larger error in the LSTR and hence for studies based on LSTR estimation, lower - resolution datasets like ERA-Interim should be used only after validation with measured data especially in the regions where comparable wind-seas and swells exist. The studies indicate that there is a large variation in the gross LSTR within 440 km stretch along the central west coast of India. In this study, the relative contribution of wind-seas and swells on LSTR are specifically examined. All previous studies have focused on the integral wave parameters than the wind-seas and swells. The annual gross LSTR based on integral wave parameters is only 58% of that considering the wind-seas and swells separately. In regions where there is large difference in the direction of the wind-seas and swells, considering the integral parameters will lead to errors in the LSTR estimate.

**Acknowledgments:** The authors gratefully acknowledge the support of the Council of Scientific & Industrial Research, New Delhi to conduct this research. The ERA-I data used in this study are available from the ECMWF data server: <https://apps.ecmwf.int/datasets/data/interim-full-daily/levtype=sfc/>. The wave data used for the model validation are from the project funded by Earth System Science Organization, Ministry of Earth Sciences, Government of India and is available on request for joint research work. Director, CSIR-NIO, Goa encouraged to carry out the study. We thank Jai Singh, P.R.Shanas, T.R.Anoop, Naseef Muhammad for the help provided during the data collection. We thank the three reviewers for the suggestions which improved the scientific content of this paper. This work forms part of the Ph.D. thesis of the first author registered at Bharathidasan University and NIO contribution No. is xxxx.

## References

1. Dean, R.G., Dalrymple, R.A. Coastal Processes - With Engineering Applications. Cambridge Univ. Press. **2002** ; DOI: 10.1017/CBO9780511754500.
2. Zhang, S., Jia, Y., Zhang, Y., Shan, H. Influence of seepage flows on the erodibility of fluidized silty sediments: parameterization and mechanisms. *J. Geophys. Res. Ocean.* **2018** ; DOI: 10.1002/2018JC013805
3. Pilkey, O.H., Cooper, J.A.G. Are natural beaches facing extinction? *J. Coast. Res.* **2014**, 70, 431–436. DOI: 10.2112/SI70-073.1

4. Shanass, P.R., Sanil Kumar, V. Coastal processes and longshore sediment transport along Kundapura coast, central west coast of India. *Geomorphology*. **2014**, 214, 436–451; DOI: 10.1016/j.geomorph.2014.02.027
5. Bergillos, R.J., Rodríguez-Delgado, C., Ortega-Sánchez, M. Advances in management tools for modeling artificial nourishments in mixed beaches. *J. Mar. Syst.* **2017**,172,1-13; DOI: 10.1016/j.jmarsys.2017.02.009
6. Bergillos, R.J., López-Ruiz, A., Principal-Gómez, D., Ortega-Sánchez, M. An integrated methodology to forecast the efficiency of nourishment strategies in eroding deltas. *Sci. Total Environ.* **2018**, 613-614, 1175-1184; DOI: 10.1016/j.scitotenv.2017.09.197
7. López-Ruiz, A., Solari, S., Ortega-Sánchez, M., Losada, M. A simple approximation for wave refraction - Application to the assessment of the nearshore wave directionality. *Ocean Model.* **2015**, 96, 324–333; DOI: 10.1016/j.ocemod.2015.09.007
8. Bergillos, R.J., López-Ruiz, A., Ortega-Sánchez, M., Masselink, G., Losada, M.A. Implications of delta retreat on wave propagation and longshore sediment transport - Guadalfeo case study (southern Spain). *Mar. Geol.*, 2016, 382,1-16 ; DOI: 10.1016/j.margeo.2016.09.011
9. Bergillos, R.J., Masselink, G., Ortega-Sánchez, M. Coupling cross-shore and longshore sediment transport to model storm response along a mixed sand-gravel coast under varying wave directions. *Coast. Eng.* **2017**,129, 93-104; DOI: 10.1016/j.coastaleng.2017.09.009
10. Watt, G.M. A study of sand movement at South Lake Worth Inlet, Florida, U.S. Army Corps of Engineers, Beach Erosion Board, Technical Memo. **1953**, 42.
11. Caldwell, J.M. Wave action and sand transport near Anaheim Bay, Calif., U.S. Army Corps of Engineers, Beach Erosion Board, Technical Memo. **1956**, 68.
12. Ingle, J. C. Jr. The movement of beach sand, *Developments in Sedimentology*. 1966
13. Komar, P.D., Inman, D.L. Longshore sand transport on beaches. *J. Geophys. Res.* **1970**, 75, 5914–5927.
14. Smith, E.R., Wang, P., Ebersole, B.A., Zhang, J. Dependence of Total Longshore Sediment Transport Rates on Incident Wave Parameters and Breaker Type. *J. Coast. Res.* **2009**, 253, 675–683; DOI:10.2112/07-0919.1
15. USACE. Shore Protection Manual. Coastal Engineering Research Center (CERC). 1984
16. Chempalayil, S.P., Kumar, V.S., Dora, G.U., Johnson, G. Near shore waves, long-shore currents and sediment transport along micro-tidal beaches, central west coast of India. *Int. J. Sediment Res.* **2014**, 29, 402–413; DOI: 10.1016/S1001-6279(14)60054-8
17. Walton Jr, T.L., Bruno, R.O. Longshore Transport at a Detached Breakwater , Phase II. *J. Coast. Res.* **1989**, 5, 679–691.
18. Kamphuis, J.W. Alongshore transport of sand, Proc. 28, Coastal Engineering Conference, ASCE. **2002**, 2478–2490.

19. Samaras, A. G., Koutitas, C. G. Comparison of three longshore sediment transport rate formulae in shoreline evolution modeling near stream mouths Ocean Eng. **2014**, 92, 255-266.
20. Bayram, A., Larson, M., Hanson, H. A new formula for the total longshore sediment transport rate. Coast. Eng. **2007**, 54, 9, 700–710.
21. Kumar, V.S., Shanas, P.R., Dora, G.U., Glejin, J., Philip, S. Longshore sediment transport in the surf zone based on different formulae: a case study along the central west coast of India. J. Coast. Conserv. **2017**, 21, 1–13; DOI: 10.1007/s11852-016-0462-8
22. Baba, M., Dattatri, J., Abraham, S. Ocean wave spectra off Cochin, west coast of India Indian Journal of Marine Sciences. **1989**, 18, 106–112.
23. Vethamony, P., Aboobacker, V.M., Menon, H.B., Kumar, K.A., Cavaleri, L. Superimposition of wind seas on pre-existing swells off Goa coast. J. Mar. Syst. **2011**, 87, 47–54; DOI: 10.1016/j.jmarsys.2011.02.024
24. Kumar, V.S., Anand, N.M., Ashok, K., Mandal, S. Multi peakedness and Groupiness of Shallow Water Waves Along Indian Coast. J. Coast. Res. **2014**, 19, 1052–1065.
25. Amrutha, M.M., Sanil Kumar, V., Sharma, S., Singh, J., Gowthaman, R., Kankara, R.S. Characteristics of shallow water waves off the central west coast of India before, during and after the onset of the Indian summer monsoon. Ocean Eng. **2015**, 107, 259–270; DOI: 10.1016/j.oceaneng.2015.07.061.
26. George, J., Sanil Kumar, V., Victor, G., Gowthaman, R. Variability of the local wave regime and the wave-induced sediment transport along the Ganpatipule coast, eastern Arabian Sea. Reg. Stud. Mar. Sci. **2019**, 100759; DOI: 10.1016/j.rsma.2019.100759
27. Noujas, V., Kankara, R.S., Rasheed, K. Estimation of Longshore Sediment Transport Rate for a Typical Pocket Beach Along West Coast of India. Mar. Geod. **2018**; DOI: 10.1080/01490419.2017.1422818
28. Dora, G.U., Kumar, V.S., Vinayaraj, P., Philip, C.S., Johnson, G. Quantitative estimation of sediment erosion and accretion processes in a micro-tidal coast. Int. J. Sediment Res. **2014**, 29, 218–231; DOI: 10.1016/S1001-6279(14)60038-X
29. Sanil Kumar, V., Pathak, K.C., Pednekar, P., Raju, N.S.N., Gowthaman, R. Coastal processes along the Indian coastline. Curr. Sci. **2006**, 91, 530–536.
30. Amrutha, M.M., Sanil Kumar, V., Singh, J. Changes in nearshore waves during the active sea/land breeze period off Vengurla, central west coast of India. Ann. Geophys. **2016**, 34, 215–226; DOI: 10.5194/angeo-34-215-2016
31. Gawali, P.B., Basavaiah, N., Hanamgond, P.T. Mineral Magnetic Properties of Sediments of Beaches, Redi–Vengurla Coast, Central West Coast of India: A Seasonal Characterization and Provenance Study. J. Coast. Res. **2010**, 263, 569–579; DOI: 10.2112/08-1111.1
32. Herlekar, M.A., Sukhtankar., R.K. Morphotectonic studies along the Part of Maharashtra coast, India. Int. J. Earth Sci. Eng. **2011**, 4, 61–83.

33. Davies L. J. A morphogenic approach to world shorelines. *Zeitschrift fur Geomorphol.* **1964**, 8, 127–142.
34. Short, A.D. Coastal processes and beaches. *Nat. Educ. Knowl.* **2012**, 3, 15.
35. Chandramohan, P., Anand, N.M., Nayak, B.U. Surfzone dynamics of Konkan coast, India. *Oceanography of the Indian Ocean.* **1992**.
36. National Hydrographic Office, Dehradun, India. *India-West coast.* **2004**.
37. Folk, R.L., Ward, W.C. Brazos River bar [Texas]; a study in the significance of grain size parameters. *J. Sediment. Res.* **1957**, 27, 3–26; DOI:10.1306/74D70646-2B21-11D7-8648000102C1865D
38. Blott, S.J., Pye, K. Gradistat: A grain size distribution and statistics package for the analysis of unconsolidated sediments. *Earth Surf. Process. Landforms.* **2001**, 26, 1237–1248; DOI: 10.1002/esp.261
39. *Hydraulics, W.L.D. Delft3D User Manual.* **2006**
40. Holthuijsen, L. H., Booij, N., Ris, R. C. A spectral wave model for the coastal zone. **1993** In *Ocean Wave Measurement and Analysis.* ASCE. 630-641
41. López-Ruiz, A., Bergillos, R. J., Ortega-Sánchez, M. The importance of wave climate forecasting on the decision-making process for nearshore wave energy exploitation. *Appl. Energy.* **2016**, 182, 191-203.
42. George, J., Sanil Kumar, V. Long-term variations in nearshore wave climate and littoral drift at Ganpatipule coast, eastern Arabian Sea and its link to Pacific climate variability. *J. Geophys. Res. C Ocean.* **2019**, 124; DOI:10.1029/2018JC014900
43. Hasselmann, K. et al., Measurements of Wind-Wave Growth and Swell Decay during the Joint North Sea Wave Project (JONSWAP). *Ergnzungsh. zur Dtsch. Hydrogr. Zeitschrift R.* **1973**, 8–12.
44. Battjes, J.A., Stive, M. J. F. Calibration and verification of a dissipation model for random breaking waves. *J. Geophys. Res. Ocean.* **1985**,90,5, 9159–9167.
45. Eldeberky, Y. Nonlinear transformation of wave spectra in the nearshore zone. *Oceanogr. Lit. Rev.* **1997**, 4,44, 297.
46. Portilla, J., Ocampo-Torres, F.J., Monbaliu, J. Spectral partitioning and identification of wind sea and swell. *J. Atmos. Ocean. Technol.* **2009**; DOI: 10.1175/2008JTECHO609.1
47. Dee, D.P., Uppala, S.M., Simmons, A.J., Berrisford, P., Poli, P., Kobayashi, S., Andrae, U., Balmaseda, M.A., Balsamo, G., Bauer, P., Bechtold, P., Beljaars, A.C.M., van de Berg, L., Bidlot, J., Bormann, N., Delsol, C., Dragani, R., Fuentes, M., Geer, A.J., Haimberger, L., Healy, S.B., Hersbach, H., Hólm, E. V., Isaksen, L., Kållberg, P., Köhler, M., Matricardi, M., McNally, A.P., Monge-Sanz, B.M., Morcrette, J.J., Park, B.K., Peubey, C., de Rosnay, P., Tavolato, C., Thépaut, J.N., Vitart, F. The ERA-Interim reanalysis: Configuration and performance of the data assimilation system. *Q. J. R. Meteorol. Soc.* **2011**, 137, 553–597; DOI: 10.1002/qj.828

48. Kumar, V.S., Pednekar, P., Chandramohan, P., Kumar, K., Gowthaman, R. Longshore currents and sediment transport along Kannirajapuram Coast, Tamilnadu, India. *J. Coast. Res.* **2000**, 16, 247–254.
  49. Amrutha, M.M., Kumar, V.S., George, J. Observations of long-period waves in the nearshore waters of central west coast of India during the fall inter-monsoon period. *Ocean Eng.* **2017**, 131, 244–262; DOI: 10.1016/j.oceaneng.2017.01.014
  50. Sanil Kumar, V., Sajiv Philip, C., Balakrishnan Nair, T.N. Waves in shallow water off west coast of India during the onset of summer monsoon. *Ann. Geophys.* **2010**, 28, 817–824; DOI: 10.5194/angeo-28-817-2010
  51. Chandramohan, P., Sanil Kumar, V., Nayak, B. U., and Pathak, K. Variation of longshore current and sediment transport along the south Maharashtra coast, west coast of India, *Indian J. Mar. Sci.* **1993**, 22, 115–118.
  52. Chandramohan, P., Nayak, B. U. Longshore sediment transport model for the Indian west coast. *J. Coast. Res.* **1992**, 8, 4, 775–787.
  53. Chandramohan P., Sanil Kumar V, Nayak, B. U., Pathak, K. C. Variation of longshore current and sediment transport along the south Maharashtra coast, west coast of India. *Indian J. Mar. Sci.* **1993**, 22, 2, 115–118.
  54. Anjali Nair, M., Sanil Kumar, V., Amrutha, M.M., Murty, V.S.N. Features of locally and remotely generated surface gravity waves in the inner-shelf region of northwestern Bay of Bengal. *Int. J. Climatol.* **2019**, 39, 1644-1664; DOI: 10.1002/joc.5907
  55. Kunte, P.D., Wagle, B.G. Littoral transport studies along west coast of India - A review. *Indian J. Mar. Sci.* **2001**, 30, 57-64
  56. Uppala, S.M., Kållberg, P.W., Simmons, A.J., Andrae, U., da Costa Bechtold, V., Fiorino, M., Gibson, J.K., Haseler, J., Hernandez, A., Kelly, G.A., Li, X., Onogi, K., Saarinen, S., Sokka, N., Allan, R.P., Andersson, E., Arpe, K., Balmaseda, M.A., Beljaars, A.C.M., van de Berg, L., Bidlot, J., Bormann, N., Caires, S., Chevallier, F., Dethof, A., Dragosavac, M., Fisher, M., Fuentes, M., Hagemann, S., Hólm, E., Hoskins, B.J., Isaksen, L., Janssen, P.A.E.M., Jenne, R., McNally, A.P., Mahfouf, J.F., Morcrette, J.J., Rayner, N.A., Saunders, R.W., Simon, P., Sterl, A., Trenberth, K.E., Untch, A., Vasiljevic, D., Viterbo, P., Woollen, J. The ERA-40 re-analysis. *Q. J. R. Meteorol. Soc.* **2005**. DOI: 10.1256/qj.04.176
  57. Splinter, K. D., Davidson, M. A., Golshani, A., Tomlinson R. Climate controls on longshore sediment transport. *Cont. Shelf Res.* **2012**, 48, 146–156.
  58. Harley M. D., Turner, I. L., Short A. D., Ranasinghe R. Interannual variability and controls of the Sydney wave climate. *Int. J. Climatol.* **2010**, 30, 9, 1322–1335.
  59. Chowdhury, P., Behera, M.R. Effect of long-term wave climate variability on longshore sediment transport along regional coastlines. *Prog. Oceanogr.* **2017**, 156, 145-153.
- Kumar, V.S., Naseef, T.M. Performance of ERA-interim wave data in the nearshore waters around India. *J. Atmos. Ocean. Technol.* **2015**, 32, 1257–1269; DOI: 10.1175/JTECH-D-14-00153.1



**Table 1.** Longshore sediment transport rate along the west coast of India

Location	Net sediment transport rate ( $10^6$ m <sup>3</sup> /y)	Gross sediment transport rate ( $10^6$ m <sup>3</sup> /y)	Data used, period and method used	Formula used	Reference
Maharastra Ganpatipule	0.08 0.01 0.05	0.23 0.04 0.19	Measured wave data (2011-2016), Delft 3D model	CERC Kamphuis Walton & Bruno	[26]
Maharashtra Vengurla	0.008	0.11	Measured wave data Jan –Dec (2015), LITDRIFT Model	-	[27]
Karnataka Karwar	0.04	0.14	Measured wave data, SWAN wave model Feb 2009-Jan 2010	Kamphuis	[28]
Karnataka Pavinkurve	0.46 0.29 0.20	0.7 0.4 0.4	Measured wave data, REFDIF-I wave model & Empirical equation Jan-Dec(2009)	CERC Walton&Bruno Komar	[16]
Kasargod	0.47 0.30 0.18	0.7 0.5 0.2		CERC Walton&Bruno Komar	
Karnataka Kundapura	0.137 0.178 0.163 0.125	0.334 0.349 0.310 0.343	Measured wave data, Delft-3D wave model & Empirical equation Jan-Dec(2011)	CERC Kamphuis Walton&Bruno Komar	[4]
Karnataka Malpe	1.12 0.82 0.33 0.89	1.26 0.92 0.35 1.01	Measured wave data, Delft-3D wave model & Empirical equation Jan-Dec(2009 & 2011)	CERC Walton&Bruno Kamphuis Komar	[21]

**Table 2.** Monthly average of significant wave height, mean wave period and mean wave direction of swell measured at 15-m water depth for four years

Month	Swell											
	H <sub>s</sub> (m)				Wave period (s)				Direction (deg)			
	2014-2015	2015-2016	2016-2017	2017-2018	2014-2015	2015-2016	2016-2017	2017-2018	2014-2015	2015-2016	2016-2017	2017-2018
Sep	1.01	0.80	1.13	0.88	8.8	9.4	8.8	8.8	245	237	249	242
Oct	0.52	0.50	0.39	0.42	10.0	10.6	10.4	10.2	229	224	225	223
Nov	0.35	0.37	0.39	0.28	11.1	10.5	11.6	11.0	223	223	222	221
Dec	0.27	0.28	0.25	0.45	10.8	10.9	11.1	10.8	219	219	212	225
Jan	0.32	0.28	0.27	0.24	11.6	11.7	11.5	11.0	225	216	219	218
Feb	0.27	0.26	0.32	0.26	11.1	10.6	10.4	11.5	223	224	224	215
Mar	0.41	0.35	0.32	0.31	11.5	11.9	11.7	10.9	224	224	225	219
Apr	0.40	0.46	0.34	0.38	11.1	11.1	10.8	11.1	221	223	221	216
May	0.47	0.89	0.71	0.69	10.7	10.0	10.5	10.0	225	235	230	226
Jun	1.80	1.78	1.90	1.79	9.3	9.5	9.4	9.2	245	249	253	251
Jul	1.54	2.0	1.87	2.23	8.9	9.6	9.4	9.7	252	251	253	250
Aug	1.18	1.60	1.42	1.43	8.8	8.7	8.9	8.8	250	252	250	253

**Table 3.** Monthly average of significant wave height, mean wave period and mean wave direction of wind-sea measured at 15-m water depth for four years

Month	Wind-sea											
	H <sub>s</sub> (m)				Wave period (s)				Direction (deg)			
	2014-2015	2015-2016	2016-2017	2017-2018	2014-2015	2015-2016	2016-2017	2017-2018	2014-2015	2015-2016	2016-2017	2017-2018
Sep	0.71	0.57	0.74	0.57	3.7	3.8	3.8	3.7	263	265	256	263
Oct	0.31	0.39	0.44	0.38	3.4	3.5	3.7	3.6	265	244	283	261
Nov	0.25	0.31	0.21	0.29	3.1	3.4	3.1	3.4	279	261	285	292
Dec	0.32	0.34	0.29	0.42	3.3	3.3	3.3	3.4	274	278	278	266
Jan	0.42	0.36	0.34	0.40	3.5	3.4	3.3	3.5	295	291	293	293
Feb	0.43	0.49	0.42	0.36	3.4	3.4	3.4	3.4	294	292	282	288
Mar	0.44	0.46	0.48	0.44	3.4	3.4	3.5	3.4	291	289	290	284
Apr	0.44	0.55	0.46	0.42	3.2	3.4	3.4	3.2	292	291	283	289
May	0.57	0.63	0.52	0.57	3.5	3.4	3.4	3.4	283	273	273	270
Jun	1.02	0.93	0.96	0.93	3.8	3.9	4.0	3.9	246	254	250	251
Jul	1.02	1.03	1.01	1.17	3.7	4.01	3.9	3.9	253	252	251	250
Aug	0.82	0.95	0.77	0.98	3.9	3.7	3.9	3.7	260	252	256	254

**Table 4.** Statistical comparison of swell and wind sea parameters between measured and model data during monsoon and non-monsoon

Season	Swell								
	Hs (m)			Mean wave period (s)			Direction (deg)		
	Bias	RMSE	R	Bias	RMSE	R	Bias	RMSE	R
Monsoon	0.08	0.28	0.84	-2	2.6	0.2	-1.7	10.2	0.55
Non- Monsoon	-0.02	0.07	0.9	-2.7	3.01	0.58	4.5	10.4	0.42
	Wind-sea								
	Hs (m)			Mean wave period (s)			Direction (deg)		
	Bias	RMSE	R	Bias	RMSE	R	Bias	RMSE	R
Monsoon	0.01	0.19	0.72	-0.38	0.69	0.31	3	12.1	0.73
Non- Monsoon	0.006	0.06	0.87	-0.63	0.75	0.58	8.2	22.1	0.55

**Table 5:** Monthly net and gross longshore sediment transport rate using the measured buoy data for four years

Month	LSTR based on buoy data							
	Gross (m <sup>3</sup> /month)				Net (m <sup>3</sup> /month)			
	2014-2015	2015-2016	2016-2017	2017-2018	2014-2015	2015-2016	2016-2017	2017-2018
September	8294	5835	5169*	6077	319	3638	1615*	-380
October	2773	3060	2092*	2253	1411	2857	395*	1967
November	1409	1698	1845	1094	1357	1393	1835	735
December	988	1144	880	2893	735	735	880	2301
January	1558	1029	964	994	632	803	578	347
February	1134	1336	1521	861	13	-263	-297	465
March	2280	1600	1485	1414	1441	1152	609	755
April	1925	2621	1696	1790	1500	1664	624	1585
May	2643	5313	4331	3258	1827	-475	1585	1009
June	19407	17309	16160	14798	15510	11444	5842	6283
July	12182	19670	13519	24256	1380	12104	2518	19993
August	10747	13577	10290	10644	113	-2432	3450	2635
Annual	65340	74192	59952	70332	26238	32620	19634	37695

\* In 2015-16 LSTR estimate in September is based on 20 days and October is 26 days

**Table 6.** Monthly net and gross longshore sediment transport rate using the measured buoy data separated into wind-sea and swell and ERA-Interim data

Month	LSTR using ERA-Interim data		LSTR due to wind-sea		LSTR due to swell		Total LSTR	
	Gross (m <sup>3</sup> /month)	Net (m <sup>3</sup> /month)	Gross (m <sup>3</sup> /month)	Net (m <sup>3</sup> /month)	Gross (m <sup>3</sup> /month)	Net (m <sup>3</sup> /month)	Gross (m <sup>3</sup> /month)	Net (m <sup>3</sup> /month)
Sep 2014	15178	6447	1813	-1503	10671	2664	12485	1160
Oct 2014	15699	15699	425	-142	4539	2958	4965	2816
Nov 2014	8179	6437	244	-194	3576	3556	3821	3362
Dec 2014	5120	1553	399	-346	2011	1858	2411	1512
Jan 2015	5615	-2419	716	-711	2911	2394	3627	1683
Feb 2015	4027	446	615	-606	1810	1461	2425	854
Mar 2015	10050	6011	762	-683	5114	4313	5876	3629
Apr 2015	10976	8816	657	-622	4402	4106	5060	3483
May 2015	7873	4621	1278	-1257	5044	3958	6323	2700
Jun 2015	29741	28918	3232	1369	27131	23018	30363	24387
July 2015	27564	-21481	2291	-1269	18432	6619	20723	5323
Aug 2015	16447	-9353	2468	-1956	13085	4124	15553	2168
Annual	156469	45695	14900	-7920	98726	61029	113632	53077

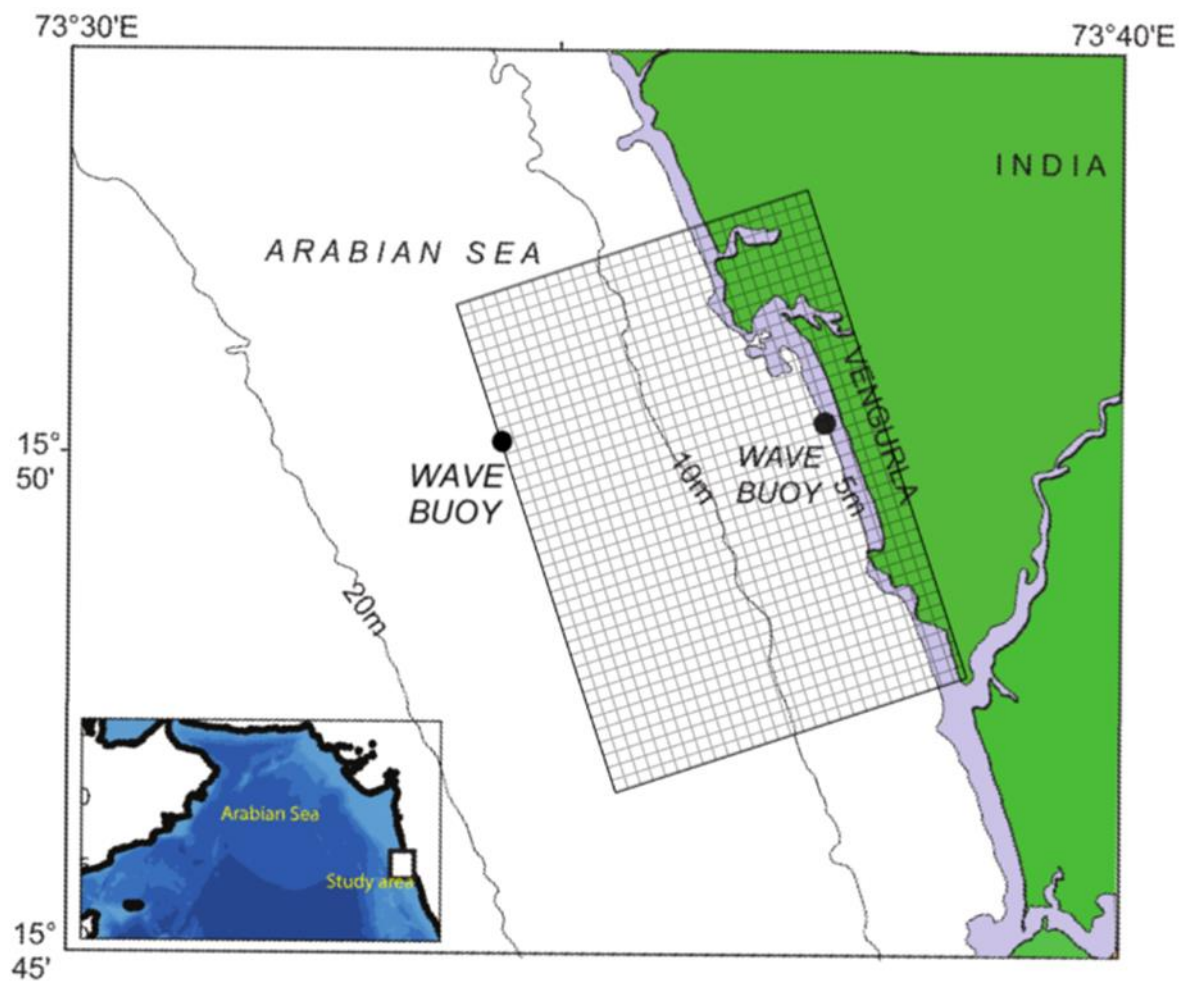


**Figure 1.** Study area in the eastern Arabian Sea showing the locations of the wave rider buoys at 15 and 5 m water depth. The rectangular box represents the model grid and its boundaries

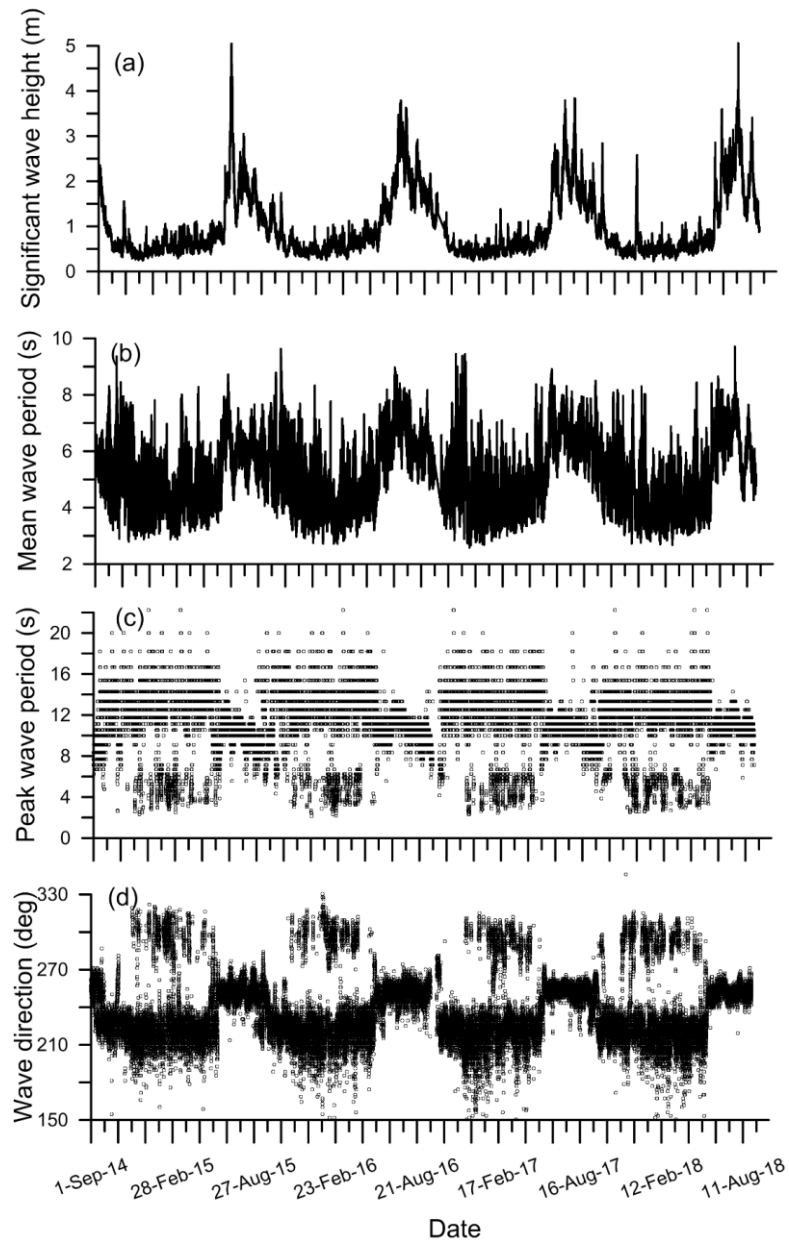


**Figure 2.** Time series plot of (a) significant wave height, (b) mean wave period, (c) peak wave period and (d) mean wave direction during 1 September 2014 to 31 August 2018 at 15 m water depth



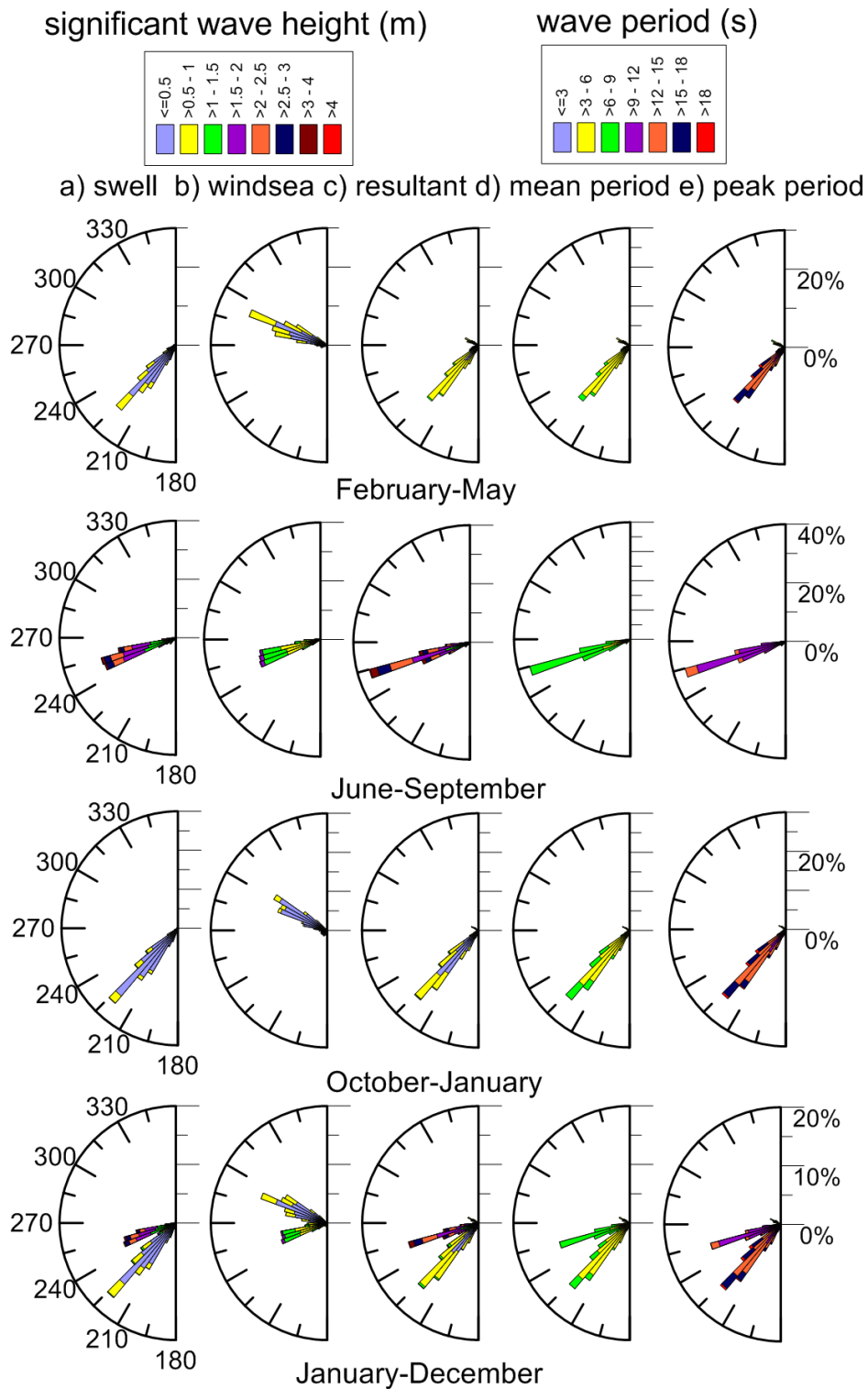


**Figure 3.** Wave rose diagram for significant wave height of a) swell, b) wind-sea and c) resultant and the right panel is for d) mean wave period and e) peak wave period in different seasons during 1 September 2014 to 31 August 2018 at 15 m water depth

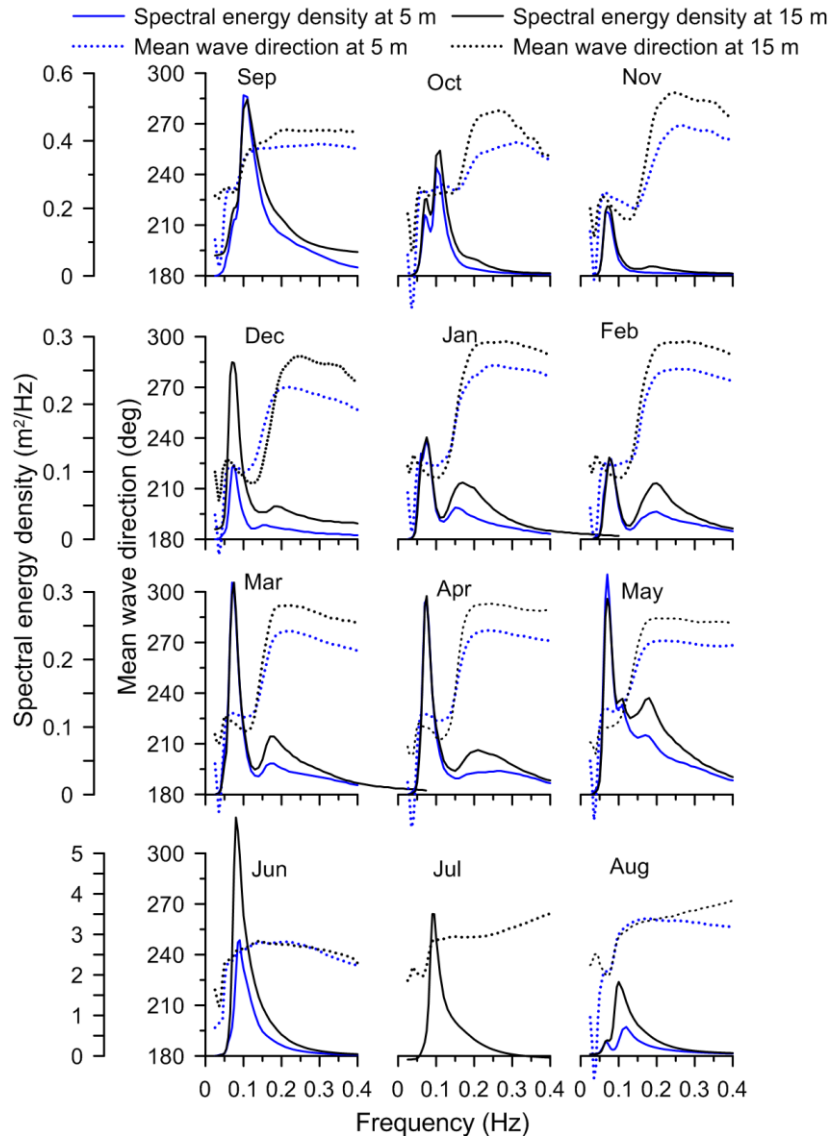


**Figure 4:** Monthly averaged wave spectrum showing the variation of spectral energy density and mean wave direction at both 15 and 5 m water depth

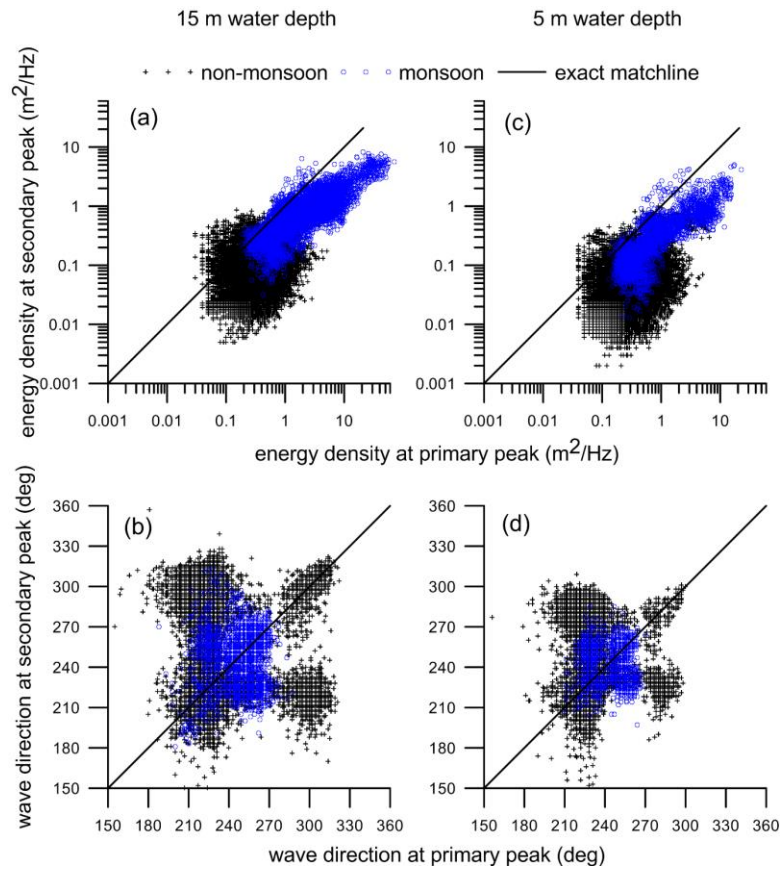


**Figure 5.** Top panel shows the scatter plot of spectral energy density at secondary peak with primary peak. Bottom panel shows the scatter plot of the wave direction at primary peak and secondary peak. The wave data during September 2014 to August 2015 at 15 m water depth is presented in (a) and (b) and that at 5 m water depth in (c) and (d)

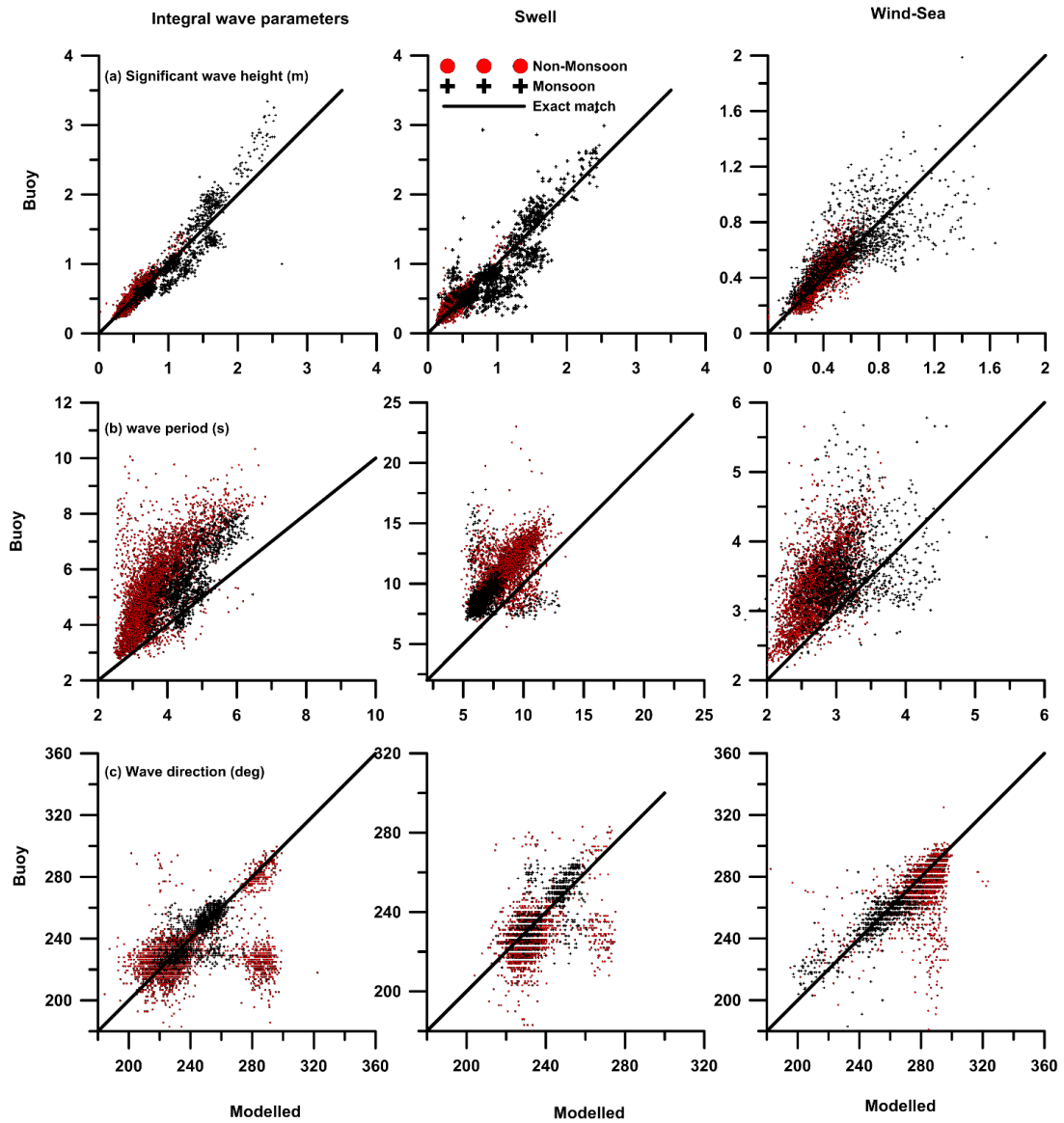


**Figure 6.** Scatter plot of a) significant wave height, b) mean wave period and c) mean wave direction for integral wave parameters, swell and wind-Sea between measured buoy data at 5 m water depth and that based on wave model

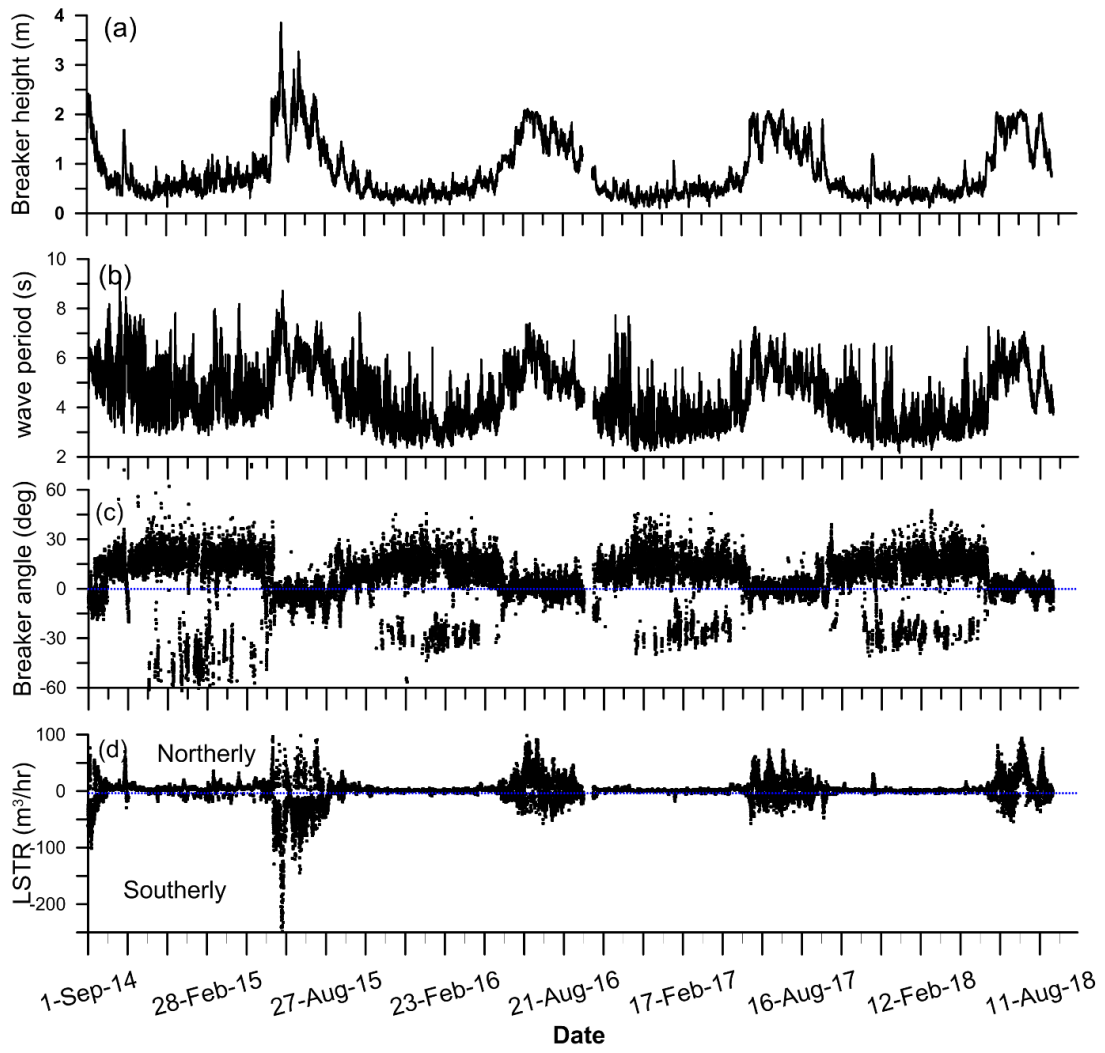


**Figure 7:** Time series plot for a) breaker height, b) wave period c) wave breaker angle, and d) longshore sediment transport rate

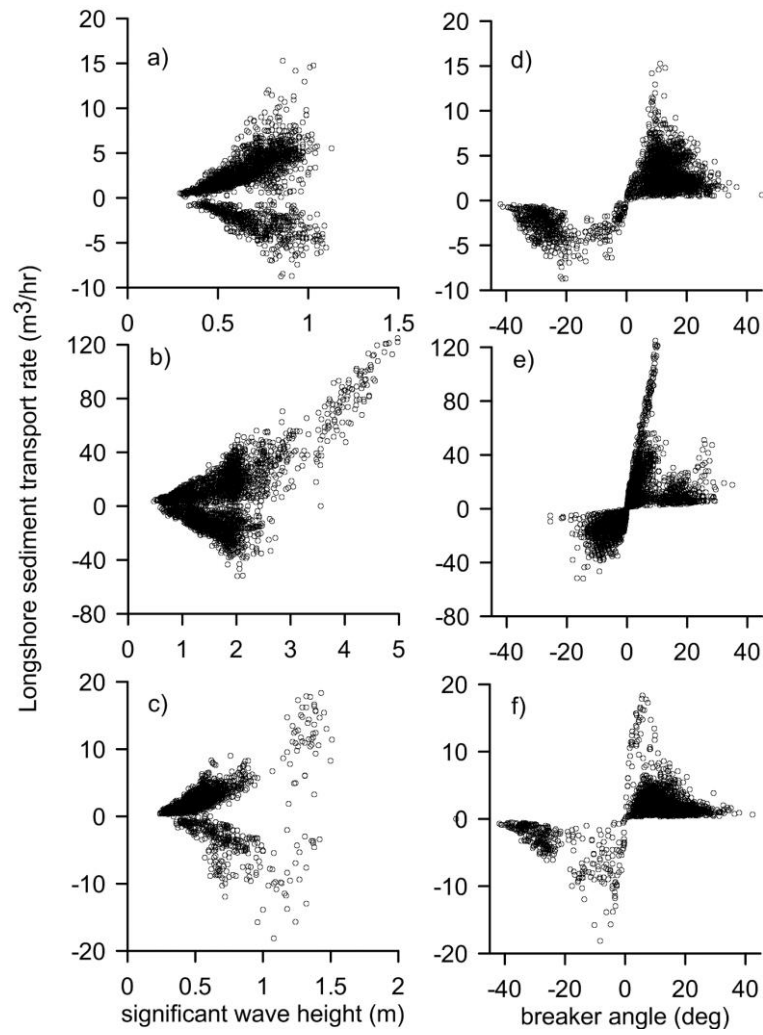


**Figure 8.** Influence of wave breaker height on the LSTR (a, b and c) and wave breaker angle on LSTR (d, e and f) in different seasons during September 2014 to August 2015. a) and d) pre-monsoon (Feb-May), b) and e) monsoon (Jun-Sept) and c) and f) post-monsoon (Oct-Jan)

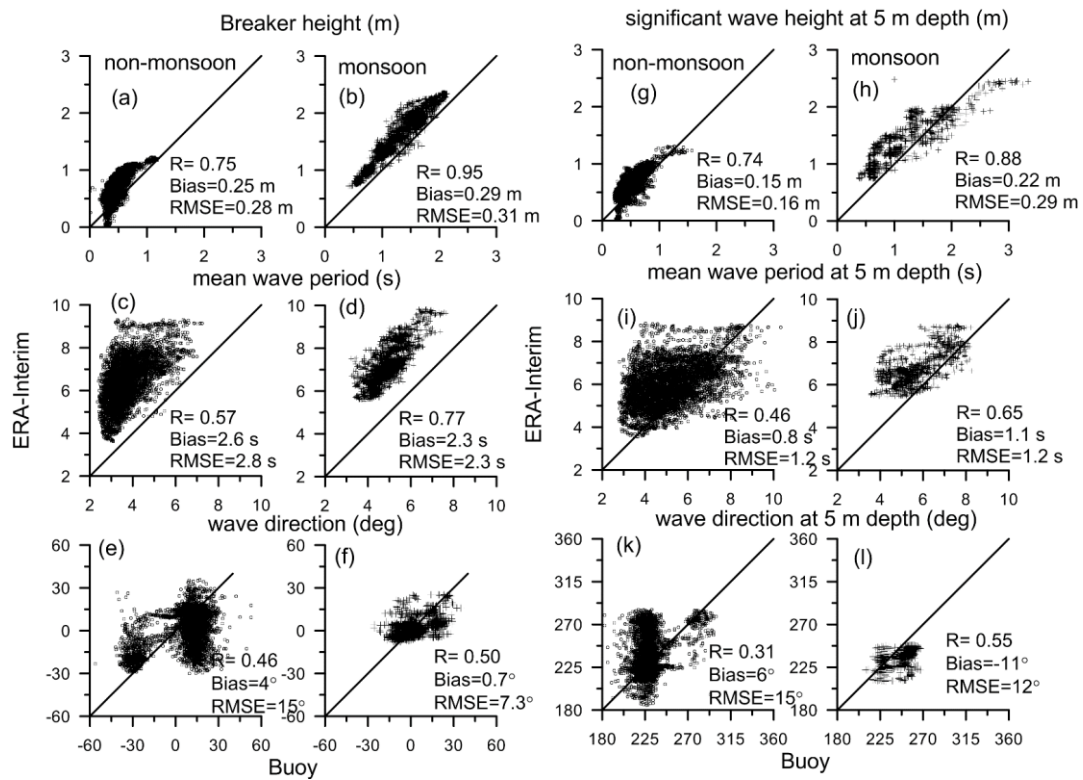


**Figure 9.** (a) to (f) shows the scatter plot between the breaker parameters from buoy measured data and ERA-Interim data. (g) to (l) shows the scatter plot between buoy measured data and ERA-Interim data at 5 m water depth

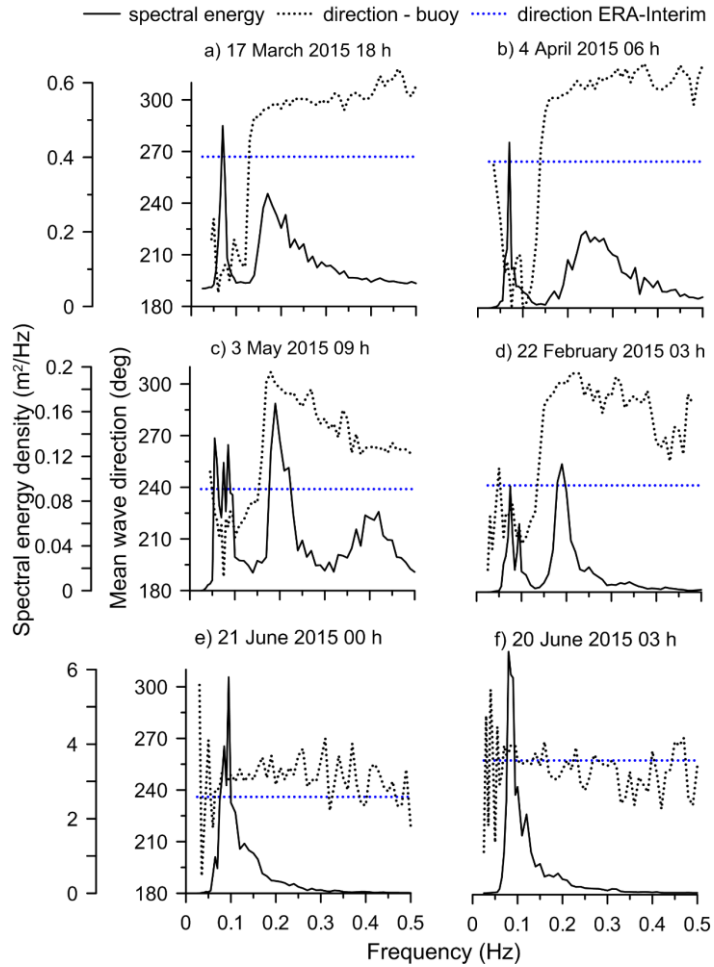


**Figure 10.** Plots showing the wave spectral energy density and mean wave direction from measured buoy data during different wave conditions along with ERA-Interim wave direction. a) and b) are swell dominated multi-peaked wave spectra, c) and d) are wind-sea dominated multi-peaked wave spectra and e) and f) are single peaked spectra during the monsoon.